MCB
Journals.ASM.org

RMI1 Promotes DNA Replication Fork Progression and Recovery from Replication Fork Stress

Jay Yang,[a] Lara O'Donnell,[b] Daniel Durocher,[b,c] and Grant W. Brown[a]

Department of Biochemistry and Donnelly Centre for Cellular and Biomolecular Research, University of Toronto, Toronto, Ontario, Canada[a]; Samuel Lunenfeld Research Institute, Mount Sinai Hospital, Toronto, Ontario, Canada[b]; and Department of Molecular Genetics, University of Toronto, Toronto, Ontario, Canada[c]

RMI1 is a member of an evolutionarily conserved complex composed of BLM and topoisomerase IIIα (TopoIIIα). This complex exhibits strand passage activity *in vitro*, which is likely important for DNA repair and DNA replication *in vivo*. The inactivation of RMI1 causes genome instability, including elevated levels of sister chromatid exchange and accelerated tumorigenesis. Using molecular combing to analyze DNA replication at the single-molecule level, we show that RMI1 is required to promote normal replication fork progression. The fork progression defect in RMI1-depleted cells is alleviated in cells lacking BLM, indicating that RMI1 functions downstream of BLM in promoting replication elongation. RMI1 localizes to subnuclear foci with BLM and TopoIIIα in response to replication stress. The proper localization of the complex requires a BLM-TopoIIIα-RMI1 interaction and is essential for RMI1 to promote recovery from replication stress. These findings reveal direct roles of RMI1 in DNA replication and the replication stress response, which could explain the molecular basis for its involvement in suppressing sister chromatid exchange and tumorigenesis.

The fidelity of DNA replication, which is essential for faithfully transmitting genetic information from one generation to the next, is challenged by a broad spectrum of obstacles encountered by replication forks during replication elongation (27). These obstacles occur naturally from stable protein-DNA complexes, repeated sequences forming secondary structures, or collisions between replication and transcription (27). Replication forks can also be impeded by exogenous agents, for example, chemicals that damage the DNA template or that inhibit DNA polymerases (48). Eukaryotic cells have an elaborate DNA replication checkpoint pathway to stabilize the replication machinery at stalled forks, enabling replication to resume once the obstacles are removed (3). However, under conditions of a prolonged inhibition of replication, stalled replication forks can collapse, resulting in the dissociation of the replisome from sites of nucleotide incorporation (28). Unprotected single-strand DNA (ssDNA) gaps at collapsed replication forks can be processed illegitimately into double-stranded breaks (DSBs) (28). Under such conditions, homologous recombination genes are required to repair collapsed replication forks and to restart DNA replication (33).

BLM is a member of the RecQ family of DNA helicases that safeguards genome integrity (24). Bloom's syndrome (BS), which arises from biallelic mutations in the *BLM* gene, is characterized by an early onset of cancer development (21). The hallmark of BS cells is a 10-fold elevation in the frequency of sister chromatid exchanges (SCEs) (7), suggesting an antirecombinogenic role of BLM. Consistent with this idea, the deletion of *SGS1*, the BLM homolog in *Saccharomyces cerevisiae*, causes elevated levels of homologous recombination and gross chromosomal rearrangements (19, 32, 53, 57). Human cells lacking BLM display elevated levels of RAD51 and Ku70 foci, indicative of the activation of homologous recombination and nonhomologous-end-joining pathways (20, 37). Therefore, BLM maintains genome integrity, at least in part, by suppressing illegitimate recombination events.

BLM preserves replication fork stability during DNA replication. BLM interacts with and stimulates the enzymatic activities of DNA polymerase δ and FEN1 endonuclease, both of which are components of the replication machinery (43, 44, 51). BS cells exhibit a reduced replication fork rate and an increased frequency of fork pausing (36), suggesting that BLM participates in normal replication progression. BLM is also required for cell survival in response to replication inhibition (17, 18, 30). During replication stress, BLM is recruited to damaged replication forks (15, 16, 37) and is phosphorylated by the replication checkpoint kinase ATR (17). During recovery from replication stress, many active replication forks fail to resume replication in BS cells (18), indicating that BLM is required to stabilize stalled replication forks. The association of DNA polymerases α and ϵ with stalled replication forks is severely compromised after the hydroxyurea (HU) arrest of yeast cells lacking Sgs1 and the ATR homolog Mec1 (11). Together, these data support a model in which BLM mediates a checkpoint response to stabilize the replication machinery at stalled forks, thereby preventing replisome dissociation and an irreversible fork collapse.

BLM functions in concert with topoisomerase IIIα (TopoIIIα) to control recombination events (29, 34). TopoIIIα belongs to the type IA family of topoisomerases (8). This family of topoisomerases, including *S. cerevisiae* Top3, modulates DNA topology via an enzyme-bridging mechanism by making transient single-stranded nicks at single-stranded DNA gaps (9). The TopoIIIα-interacting domain of BLM is required for the suppression of SCEs in BS cells (26), suggesting that TopoIIIα plays an antirecombinogenic role with BLM. Biochemically, TopoIIIα catalyzes the decatenation of single-stranded DNA catenanes (58). The decatenase activity of

Received 27 February 2012 **Returned for modification** 18 March 2012
Accepted 18 May 2012
Published ahead of print 29 May 2012
Address correspondence to Grant W. Brown, grant.brown@utoronto.ca.
Supplemental material for this article may be found at http://mcb.asm.org/.

doi:10.1128/MCB.00255-12

TopoIIIα, coupled with the helicase activity of BLM, is uniquely suited to dissolve double-Holliday-junction (DHJ) structures, which arise during homologous recombination, via a strand passage mechanism to prevent the exchange between flanking sequences (55). The resolution of recombination intermediates via this strand passage activity of BLM-TopoIIIα homologs is conserved in evolution from *Escherichia coli* (47), to *S. cerevisiae* (6), to *Drosophila melanogaster* (35), to humans (55) and is presumed to mimic the *in vivo* role of BLM-TopoIIIα in the suppression of SCEs. Given that DHJ structures are intermediates that arise during homologous recombination, the conservation of the strand passage activity reflects the evolutionary importance of the RecQ helicase-topoisomerase III partnership in suppressing illegitimate recombination *in vivo*.

In eukaryotes, RMI1 is an essential member of the RecQ-topoisomerase III complex (10, 31, 59). RMI1 is a structural protein that contains a three-helix bundle domain, an OB-fold domain (OB1) at the N terminus, and a second OB-fold domain (OB2) at the C terminus (25, 50). The RMI1 N terminus is conserved from yeast to humans and is responsible for interactions with BLM and TopoIIIα (10, 39, 50). The RMI1 C terminus, which is present only in metazoans (10), interacts with RMI2 via OB2 (25, 50). The primary role of RMI1 is thought to be the resolution of recombination intermediates in concert with BLM and TopoIIIα. Biochemically, RMI1 stimulates TopoIIIα activity in DHJ dissolution and in ssDNA decatenation (38, 54, 58). Stimulation requires a physical interaction between RMI1 and TopoIIIα (39, 50, 58). At the cellular level, RMI1 is required for the recruitment of BLM to nuclear foci in response to DNA damage (59). Moreover, cells that are depleted of RMI1 show reduced viability and elevated levels of SCEs (59), the hallmark of BS cells. These data indicate that RMI1 functions with BLM and TopoIIIα to suppress illegitimate recombination.

Considerable biochemical evidence indicates a role for RMI1 in resolving recombination intermediates in concert with BLM and TopoIIIα. These recombination intermediates could arise during the processing of stalled replication forks or during the repair of double-strand breaks after a fork collapse. Given that BLM is intimately involved in maintaining replication fork integrity, we explore the possibility that RMI1 functions in DNA replication *in vivo*. We show that RMI1 localizes to subnuclear foci with BLM and TopoIIIα, both spontaneously and during replication stress. The localization of RMI1 is dependent on the presence of BLM and TopoIIIα. RMI1 functions with BLM to ensure normal replication elongation and is required for recovery from aphidicolin-induced replication stress. A proper response to replication stress requires the physical interactions between RMI1 and TopoIIIα. Our data indicate that RMI1 maintains genome integrity by promoting normal DNA replication elongation and by facilitating recovery from replication stress in concert with TopoIIIα.

MATERIALS AND METHODS

Chemicals. Doxycycline (catalog number D9891; Sigma) was dissolved in distilled water (dH_2O) to 5 mg/ml and stored at −20°C. A final working concentration of 5 μg/ml was used, unless indicated otherwise. HU (catalog number H8627; Sigma) was dissolved in dH_2O to 2 M and stored at −20°C. Aphidicolin (catalog number A0781; Sigma) was dissolved in 100% dimethyl sulfoxide (DMSO) to 30 mM and stored at −20°C.

Antibodies. For the production of the polyclonal anti-RMI1 antibody (antibody 6534), a rabbit was immunized with four injections of full-length N-terminally His_6-tagged RMI1, and the serum was collected at day 49 of immunization. To affinity purify the serum, 5 mg of purified His_6-RMI1 was subjected to SDS-PAGE and transferred onto a nitrocellulose membrane. The membrane was blocked with 5% milk in Tris-buffered saline–Tween (TBST) before being incubated with the serum overnight at room temperature. The membrane was then washed four times with TBST, and the bound antibody was eluted in 4 M $MgCl_2$ plus 50 μg/ml bovine serum albumin (BSA). The eluate was dialyzed overnight against 10 mM Tris (pH 7.2) before being aliquoted and stored at −80°C. Anti-BLM antibody (69D) was a gift from Weidong Wang (National Institutes of Health, Baltimore, MD). Anti-BLM antibody C-18 was purchased from Santa Cruz Biotechnology. Anti-TopoIIIα antibody (D6) was a gift from Ian Hickson (University of Copenhagen). Antitubulin antibody (DM1A) was purchased from Santa Cruz Biotechnology. Anti-green fluorescent protein (GFP) antibody was a gift from Laurence Pelletier (Samuel Lunenfeld Research Institute). Anti-γH2AX antibody (JBW301) was purchased from Millipore. Anti-FLAG antibody (M2) was purchased from Sigma-Aldrich. Anti-V5 antibody (R960-25) was purchased from Invitrogen.

Cell culture. All culture media were supplemented with 10% heat-inactivated fetal bovine serum (FBS), 100 U/ml penicillin, and 100 μg/ml streptomycin. U2OS cells were cultured in McCoy's medium. U2OS FRT/TO Flip-In stable cells were cultured in McCoy's medium supplemented additionally with 200 μg/ml hygromycin B and 5 μg/ml blasticidin. HEK293 FRT/TO Flip-In stable cells were cultured in Dulbecco's modified Eagle's medium (DMEM) supplemented additionally with 1× GlutaMAX (catalog number 35050; Invitrogen), 200 μg/ml hygromycin B, and 5 μg/ml blasticidin. Transformed BLM-deficient (PSNG13) and BLM-complemented (PSNF5) fibroblasts were cultured in a minimal essential medium supplemented additionally with 1× GlutaMAX and 350 μg/ml G418 (20).

FRT/TO Flp-In stable cell lines. All U2OS and HEK293 FRT/TO Flp-In stable cell lines expressing inducible RMI1 or TopoIIIα were generated by using the Flp-In T-REx system (Invitrogen), as described previously (46).

siRNA interference. Custom small interfering RNAs (siRNAs) were purchased from Dharmacon. Sequences of siRNA oligonucleotides used in this study are listed in Table S1 in the supplemental material. The knockdown efficiency of each siRNA oligonucleotide in Table S1 was evaluated (see Fig. S1 in the supplemental material). siCTRL, an siRNA that does not have a target in the human genome, was used as a negative control. Based on this evaluation, siRMI1-1, siTOP3-3, and siBLM-1 were selected to knock down their respective protein targets in subsequent experiments, unless indicated otherwise. All experiments were performed 48 h after siRNA transfection to achieve optimal protein depletion, unless indicated otherwise.

Transfection reagents. Effectene transfection reagent (catalog number 301425; Qiagen) was used to carry out plasmid transfection to generate U2OS and HEK293 FRT/TO Flp-In stable cell lines. Lipofectamine 2000 (catalog number 11668; Invitrogen) was used to carry out plasmid transfection into HEK293 FRT/TO Flp-In stable cells for immunoprecipitation experiments and to carry out siRNA transfection in U2OS, PSNF5, and PSNG13 cells. Lipofectamine RNAiMAX (catalog number 13778; Invitrogen) was used to carry out siRNA transfection in U2OS FRT/TO Flp-In stable cells.

Plasmids. To construct plasmids for the generation of stable cell lines, the RMI1 (catalog number AK022950; NITE Biological Resource Center) and TOP3A (catalog number 6044661; Open Biosystems) genes were amplified from cDNA clones. The PCR products were digested with AscI and XhoI and cloned into the pcDNA5/FRT/TO-FLAG or pcDNA5/FRT/TO-eGFP vector to generate N-terminally FLAG- or GFP-tagged gene constructs that can be integrated into the mammalian genome by the Flp-In T-REx system (Invitrogen). To generate an RMI1-expressing con-

struct resistant to siRMI1-1 treatment, eight silent point mutations were introduced into the RMI1 sequence by QuikChange mutagenesis (Stratagene). The RMI1-LLTD and -K166A mutants were constructed by QuikChange mutagenesis, as described previously (58).

Gateway cloning technology (Invitrogen) was used to generate mammalian expression plasmids that express TopoIIIα and RMI2 for immunoprecipitation experiments. Briefly, the full-length TOP3A gene was amplified from the cDNA clone (catalog number 6044661; Open Biosystems), and RMI2 was amplified from pIRESpuro3-His6-Flag-hRmi2 (56). The PCR products were cloned into pDONR201 (Invitrogen) to make entry clones. The TOP3A and RMI2 genes were then shuttled from the entry clone to the pDEST40 (Invitrogen) destination vector to make pDEST-TOP3A-V5-6His and pDEST-RMI2-V5-6His, which express C-terminally V5-tagged TopoIIIα and RMI2.

All primers used for plasmid constructions were purchased from Integrated DNA Technologies. Their sequences are listed in Table S2 in the supplemental material. All constructs were confirmed by sequencing.

Immunoprecipitation. HEK293 stable cell lines expressing N-terminally FLAG-tagged RMI1, TopoIIIα, or RMI2 were induced with 5 μg/ml doxycycline for 24 h before being harvested. When necessary, cells were transfected with pcDNA-TopoIIIα-V5-6His or pcDNA-RMI2-V5-6His 24 h prior to doxycycline induction to express C-terminally V5-tagged TopoIIIα and RMI2. After being washed in ice-cold phosphate-buffered saline (PBS), pellets from approximately 10^7 HEK293 cells were lysed in 100 μl lysis buffer (50 mM HEPES [pH 8.0], 100 mM KCl, 2 mM EDTA, 0.5% NP-40, 10% glycerol, 0.25 mM Na-orthovanadate, 10 mM NaF, 50 mM β-glycerolphosphate [pH 7.5], 1 mM dithiothreitol [DTT], 1× Complete protease inhibitor cocktail [catalog number 11836170001; Roche], and 12 units of Benzonase nuclease [catalog number E1014; Sigma]) on ice for 30 min. The extract was clarified by centrifugation at 14,000 rpm for 20 min at 4°C, and the amount of total protein in the supernatant was measured by a Bradford assay (catalog number 23238; Pierce). The normalized supernatant (1.5 mg of total protein) was incubated with 60 μl of Dynabeads protein A (catalog number 10002D; Invitrogen) coupled to 5 μl anti-FLAG antibody (M2; Sigma-Aldrich) or to 2 μl anti-V5 antibody (R690-25; Invitrogen) overnight at 4°C. Immunoprecipitates were washed two times with lysis buffer prior to being eluted in 2× sample buffer (166 mM Tris-HCl [pH 6.8], 20% glycerol, 2% SDS, 0.006% bromophenol blue, and 20 mM DTT) and boiled at 95°C for 5 min. Proteins were resolved on 10% SDS-PAGE gels, transferred onto nitrocellulose membranes, and subjected to immunoblotting analysis with anti-TopoIIIα (D6) (1:5,000 dilution), anti-RMI1 (6534) (1:2,000 dilution), and anti-V5 (1:5,000 dilution; Invitrogen) antibodies.

Fluorescence microscopy for protein localization. U2OS cells were grown in 8-well CultureSlides (catalog number 354108; BD Falcon). Cells were fixed with 2% paraformaldehyde in PBS for 30 min and then permeabilized with 0.3% Triton X-100 in PBS for another 30 min. Cells were blocked in blocking buffer (10% donkey serum, 0.5% NP-40, and 0.5% saponin in PBS) for 30 min at room temperature. For immunostaining, cells were incubated with a primary antibody overnight at 4°C and with a secondary antibody for 2 h at room temperature. Rabbit anti-RMI1 (6534) (1:200 dilution) and goat anti-rabbit Alexa Fluor 546 (1:500; Molecular Probes)-conjugated antibodies were used to detect RMI1 foci. Goat anti-BLM (C-18) (1:150 dilution) and donkey anti-goat Alexa Fluor 546 (1:500; Molecular Probes)-conjugated antibodies were used to detect BLM foci. Mouse anti-γH2AX (JBW301) (1:5,000) and goat anti-mouse Alexa Fluor 546 (1:3,000; Molecular Probes)-conjugated antibodies were used to detect γH2AX foci. All antibodies were diluted in blocking buffer. Between each step, cells were washed three times with PBS for 5 min each. Cells were stained with 0.4 μg/ml 4′,6-diamidino-2-phenylindole (DAPI) for 20 min to visualize DNA and were mounted with ProLong Gold antifade reagent (catalog number P36934; Invitrogen). For the detection of GFP-RMI1 or GFP-TopoIIIα foci, cells were stained with DAPI and mounted with ProLong Gold directly after fixation. Confocal images were taken by using Volocity imaging software (Perkin-Elmer) controlling a Leica DMI6000 microscope with fluorescein isothiocyanate (FITC), Cy3, Texas Red, and DAPI filter sets (Quorum Technologies). The maximum *z* projections of each image containing 9 *z* slices with a 0.5-μm step size were analyzed by using CellProfiler. At least 100 nuclear foci were analyzed per sample.

Molecular combing. Asynchronous populations of cells that were 70 to 90% confluent were first labeled with 25 μM 5′-chlorodeoxyuridine (CldU) for 30 min, washed with 1× prewarmed PBS, and then labeled with 100 μM iododeoxyuridine (IdU) for another 30 min. Cells were trypsinized, pooled, and cast into 1% low-melt-grade agarose plugs (catalog number AGA101; Bioshop) to a final concentration of 5×10^6 cells/ml. The plugs were incubated in 1% *N*-lauryl sarcosyl plus 1 mg/ml proteinase K at 50°C for 72 h, with fresh proteinase K solution being added every 24 h to digest proteins. The plugs were washed in Tris-EDTA (TE) with 0.2 mM phenylmethylsulfonyl fluoride (PMSF) three times and then in TE without PMSF 3 times, for 30 min each, to remove degraded materials. Protein-free DNA plugs were incubated with 6.7 μM YOYO-1 (catalog number Y3601; Invitrogen) for 30 min at room temperature. The plugs were rinsed three times in TE before being melted at 68°C in two steps, first in 150 μl TE for 20 min and then in 2 ml 100 mM morpholineethanesulfonic acid (MES) (pH 6.0) for another 20 min. The agarose solution was then treated with β-agarase (catalog number AGA777; Bioshop) overnight at 42°C to avoid resolidification. DNA fibers were combed onto silanized coverslips (12), fixed by incubating the combed coverslips at 60°C for 90 min, and mounted onto glass slides by using Instant Krazy Glue. Coverslips were dehydrated in 70%, 90%, and 100% ethyl alcohol (EtOH) for 5 min each, consecutively. The coverslips were incubated in 1 M NaOH for 25 min, washed five times in PBS, and rinsed one time in PBS plus 0.05% Tween 20 (PBST) to denature double-stranded DNA. Coverslips were blocked in blocking buffer (PBST plus 10% BSA) for 30 min at room temperature. Next, coverslips were incubated first with mixture of anti-CldU (1:40 dilutions) (BU1/75; AbD Serotec) and anti-IdU (1:10 dilutions) (B44; BD Biosciences) antibodies, then with anti-DNA antibody (1:150 dilutions) (MAB3034; Millipore) alone, and finally with a mixture of anti-rat IgG–Alexa Fluor 488 (1:75 dilutions) (catalog number A11006), anti-mouse IgG1–Alexa Fluor 546 (1:50 dilutions) (catalog number A21123), and anti-mouse IgG2a–Alexa Fluor 647 (1:50 dilutions) (catalog number A21241) (all from Molecular Probes) antibodies. All antibodies were diluted in blocking buffer and incubated with DNA fibers in a humid chamber for 1 to 2 h at 37°C. Following each staining step, the coverslips were washed with three times with PBST for 5 min each. The coverslips were mounted with ProLong Gold antifade reagent (catalog number P36934; Invitrogen) and imaged by using an Axioskop inverted microscope with a 63× objective. Individual coverslips were blinded before image acquisition to avoid bias in the analysis. The images were processed to maximize the signal intensity, and fluorescent tracks were measured with Adobe Photoshop. Approximately 100 tracks were measured per sample, and track lengths were converted from pixels to kilobase pairs using a conversion factor based on combing λ DNA (2). Experiments were repeated at least twice. Data from independent experiments were pooled, and the distribution of track lengths was plotted as a box plot. The Mann-Whitney U test was used to compare the distributions of the track lengths.

RESULTS

RMI1 colocalizes with BLM and TopoIIIα in response to replication inhibition. To understand the role of RMI and TopoIIIα during DNA replication, we asked whether either protein formed nuclear foci in response to DNA replication inhibition. We generated U2OS stable cell lines that expressed N-terminally GFP-tagged RMI1 (GFP-RMI1), TopoIII (GFP-TopoIII), or GFP alone under the control of a doxycycline-inducible promoter (see Fig. S2A and B in the supplemental material). These cell lines were treated without drug or with 4 mM HU or 30 μM aphidicolin for 24 h before visualization by confocal microscopy. Approximately

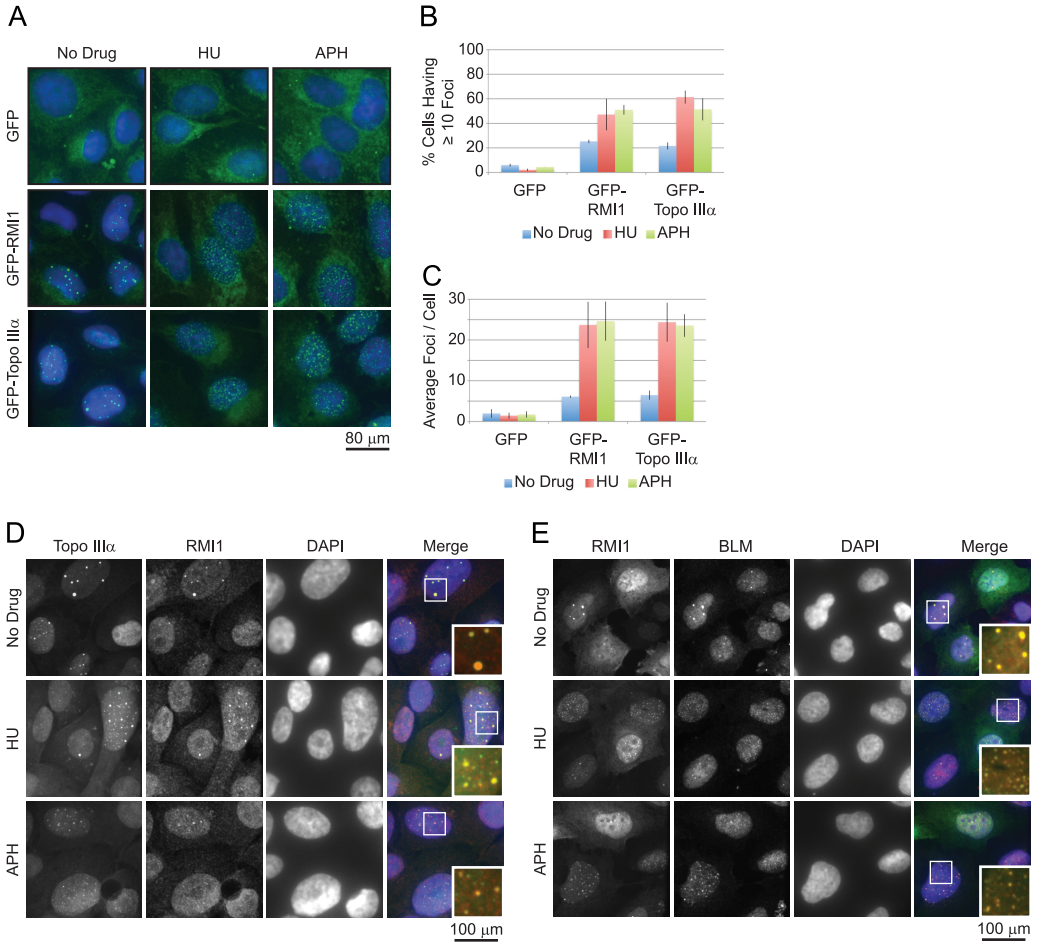

FIG 1 RMI1 and TopoIIIα form nuclear foci spontaneously and in response to replication fork stress. (A) Representative confocal microscopy images of GFP, GFP-RMI1, or GFP-TopoIIIα foci (green) in the nucleus (blue) (DAPI) in cells treated with no drug, 4 mM HU, or 30 μM aphidicolin (APH). (B and C) Images from the experiment depicted in panel A were analyzed to determine the percentage of cells that had more than 10 nuclear foci (B) or the average number of foci per cell (C). (D) A U2OS stable cell line that expresses GFP-TopoIIIα was treated with no drug, 4 mM HU, or 30 μM aphidicolin for 24 h before being subjected to indirect immunofluorescence analysis using an anti-RMI1 antibody. Representative confocal microscopy images are shown, to visualize TopoIIIα (green) or RMI1 (red) foci in the nucleus (blue) (DAPI). (E) A U2OS stable cell line that expresses GFP-RMI1 was treated with no drug, 4 mM HU, or 30 μM aphidicolin for 24 h before being subjected to indirect immunofluorescence analysis using an anti-BLM antibody. Representative confocal microscopy images are shown, to visualize RMI1 (green) or BLM (red) foci in the nucleus (blue) (DAPI).

20% of cells expressing GFP-RMI1 or GFP-TopoIIIα exhibited punctate nuclear foci even in the absence of exogenous DNA replication stress (no drug) (Fig. 1A and B). The nuclear foci formed by GFP-RMI1 and GFP-TopoIIIα intensified when DNA synthesis was interrupted (HU and aphidicolin) (Fig. 1A and B). Not only did the percentage of cells having nuclear foci increase by 2-fold, the average number of nuclear foci per cell also increased dramatically, by almost 5-fold, in response to replication inhibition (Fig. 1C). The increase in the numbers of foci per cell suggests that the enhanced formation of RMI1 and TopoIIIα foci in response to replication stress is not an indirect consequence of cell cycle arrest. These data indicate that RMI1 and TopoIIIα participate in the DNA replication stress response *in vivo*.

Since RMI1 and TopoIIIα exhibited similar nuclear localization patterns, we explored the possibility that the two proteins localize with each other. In unchallenged U2OS cells and in cells treated with replication inhibitors, we observed a strong colocalization of RMI1 and TopoIIIα foci (Fig. 1D). Moreover, we also observed a colocalization of RMI1 and BLM foci (Fig. 1E). These data are consistent with biochemical and genetic evidence showing that BLM, TopoIIIα, and RMI1 function as a complex (38, 54, 59).

RMI1 localization to nuclear foci is dependent on BLM and TopoIIIα. Using U2OS stable cell lines that expressed GFP-RMI1, we asked whether RMI1 nuclear focus formation depends on the presence of BLM or TopoIIIα. In cells that were depleted of BLM or TopoIIIα using siRNA, we observed a decrease in the ability of GFP-RMI1 to form nuclear foci (Fig. 2A and B). The reduction in numbers of RMI1 nuclear foci was not due to a reduction in the abundance of RMI1 because GFP-RMI1 was present at similar levels in all knockdowns (Fig. 2C). The reduction was evident in both unperturbed cells and cells stressed with replication inhibitors, suggesting that the response of RMI1 to endogenous DNA replication stress and to replication inhibition requires its interacting partners BLM and TopoIIIα.

TopoIIIα localization to nuclear foci is dependent on BLM and RMI1. We next asked whether TopoIIIα nuclear focus formation is dependent on the presence of BLM and RMI1. Using a

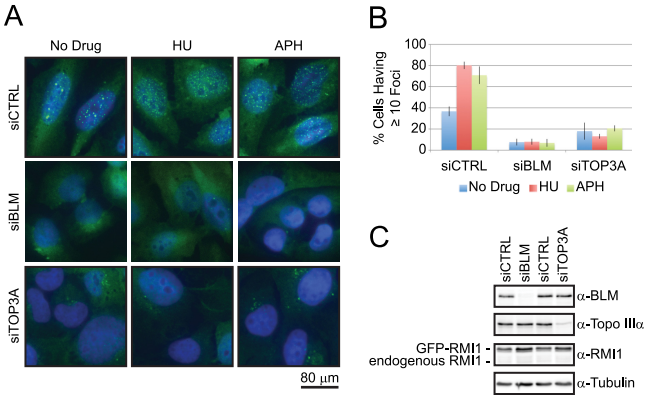

FIG 2 RMI1 nuclear focus formation is dependent on the presence of BLM and TopoIIIα. (A) Representative confocal microscopy images of RMI1 (green) foci in the nucleus (blue) (DAPI) following treatment with siCTRL, siBLM, or siTOPO3A in cells grown with no drug, 4 mM HU, or 30 μM aphidicolin for 24 h. (B) Images from the experiment depicted in panel A were analyzed to determine the percentage of cells with more than 10 RMI1 nuclear foci. (C) A U2OS stable cell line that expresses GFP-RMI1 was treated with siCTRL, siBLM, or siTOPO3A oligonucleotides for 48 h. Extracts were subjected to immunoblotting analysis, probing for BLM, TopoIIIα, and RMI1. An antitubulin antibody was included as a loading control.

U2OS stable cell line that expressed GFP-TopoIIIα, we found that the ability of GFP-TopoIIIα to form nuclear foci was severely compromised in the absence of BLM or RMI1 (see Fig. S3A and B in the supplemental material). Importantly, the reduction in numbers of TopoIIIα nuclear foci was not due to the reduction in the abundance of TopoIIIα because in the stable cell line, GFP-TopoIIIα was present at similar levels in all knockdowns (see Fig. S3C in the supplemental material). This contrasts with the decrease in endogenous TopoIIIα levels seen when RMI1 is depleted (56, 59). Therefore, TopoIIIα focus formation is dependent on its partners BLM and RMI1.

BLM localization to nuclear foci is dependent on TopoIIIα and RMI1. To study whether BLM nuclear focus formation is dependent on the presence of TopoIIIα and RMI1, we depleted TopoIIIα or RMI1 in U2OS stable cell lines that expressed GFP-RMI1 or GFP-TopoIIIα, respectively. We found that the ability of BLM to form nuclear foci was severely compromised in the absence of TopoIIIα or RMI1 (see Fig. S4A and B in the supplemental material). BLM levels were comparable in all knockdowns (see Fig. S4C in the supplemental material), suggesting that the reduction in numbers of BLM nuclear foci was not due to the reduction in the abundance of BLM. Therefore, BLM focus formation is dependent on TopoIIIα and RMI1.

RMI1 is required for normal replication fork progression. The formation of nuclear foci in the absence of exogenous replication stress suggested that RMI1 might play a role in normal DNA replication. We examined replication fork progression directly at the single-molecule level using molecular combing (2). Asynchronous U2OS cells depleted of endogenous RMI1 (Fig. 3A) were pulse-labeled with CldU (5′-chlorodeoxyuridine) and IdU (5′-iododeoxyuridine) consecutively for 30 min each. Individual DNA fibers were stretched onto silanized coverslips, and the rate of replication fork progression was calculated by expressing the length of IdU tracks as a function of time (Fig. 3B and C). We found that while replication forks moved at 1.34 kbp min^{-1} in cells treated with a control siRNA (siCTRL), they slowed to 0.94 kbp min^{-1} (siRMI1-1; $P = 2.3e{-}09$) and 1.10 kbp min^{-1} (siRMI1-2; $P = 2.0e{-}05$) in cells depleted of RMI1 (Fig. 3D), suggesting that RMI1 is required for normal replication fork progression. Since two independent siRNA oligonucleotides that target RMI1 resulted in similar phenotypes (siRMI1-1 versus siRMI1-2; $P > 0.05$), it is unlikely that the reduced DNA replication fork rate is an off-target effect. Subsequent experiments used the siRMI1-1 oligonucleotide (siRMI1).

The shorter IdU tracks observed for RMI1-deficient cells could be due to a reduced fork rate and/or frequent fork pausing. To determine whether RMI1 is required to prevent replication fork pausing, we measured the degree of asymmetry in bidirectional replication forks (Fig. 3E). Frequent fork-pausing events can lead to asymmetry in pairs of forks emanating from the same origin (13, 36, 40, 49). We found no increase in replication fork asymmetry in RMI1-depleted cells (20% in siCTRL versus 20% in siRMI1; $P > 0.05$) (Fig. 3F to H), suggesting that the frequency of fork pausing is not increased in the absence of RMI1.

The function of RMI1 in fork progression is downstream of BLM. To investigate the possibility that RMI1 functions with BLM to promote replication fork progression, we asked whether the RMI1 fork progression defect could be alleviated in the absence of BLM. We depleted RMI1 in isogenic human fibroblast cell lines that differ only in their BLM statuses ($BLM^{-/-}$, PSNG13; BLM^{+}, PSNF5 [20]) (Fig. 3I). We found that while the RMI1 depletion led to a reduction in the rate of replication fork progression in BLM^{+} cells (1.34 kbp/min for siCTRL versus 0.79 kbp/min for siRMI1; $P = 1.1e{-}15$), no significant reduction was observed for $BLM^{-/-}$ cells (1.25 kbp/min for siCTRL versus 1.10 kbp/min for siRMI1; $P = 0.045$) (Fig. 3J). These data are reminiscent of those reported previously for *S. cerevisiae*, in which many phenotypes of *rmi1*Δ mutants were suppressed by a loss of *SGS1* (10, 31), and suggest that RMI1 functions downstream of BLM in mediating normal fork progression.

The RMI1-K166A mutant is defective in interacting with members of the BLM complex. Previous biochemical studies identified two RMI1 mutants (RMI1-LLTD and RMI1-K166A) that were defective in binding to TopoIIIα (39, 58). To assay their interactions in mammalian cells, we performed coimmunoprecipitation experiments with HEK293 cell extracts from stable cell lines expressing RMI1 variants (see Fig. S2C in the supplemental material). Both the RMI1-LLTD and -K166A mutants exhibited defects in binding to endogenous BLM and TopoIIIα (Fig. 4A). Interestingly, the TopoIIIα binding of RMI1-LLTD, but not RMI1-K166A, was partially restored in HEK293 cells expressing recombinant TopoIIIα (Fig. 4B and C). Therefore, lysine 166 of RMI1 is required for BLM-TopoIIIα-RMI1 complex formation *in vivo*.

RMI2 is also a core member of the BLM complex (45, 56). However, unlike BLM and TopoIIIα, which bind to the evolutionarily conserved N terminus of RMI1, RMI2 interacts with the C terminus of RMI1 (25, 50). We repeated coimmunoprecipitation experiments with HEK293 cell extracts from stable cell lines expressing recombinant RMI1 and RMI2. We found that both the RMI1-LLTD and RMI1-K166A mutants retained RMI2 binding ability (Fig. 4D and E). However, RMI1-K166A (39 to 67% reduction) was more defective than RMI1-LLTD (no reduction) in RMI2 binding, which suggests a scenario in which the binding of BLM and TopoIIIα promotes RMI1 interactions with RMI2. Given that the RMI1-K166A mutant is more defective in BLM-

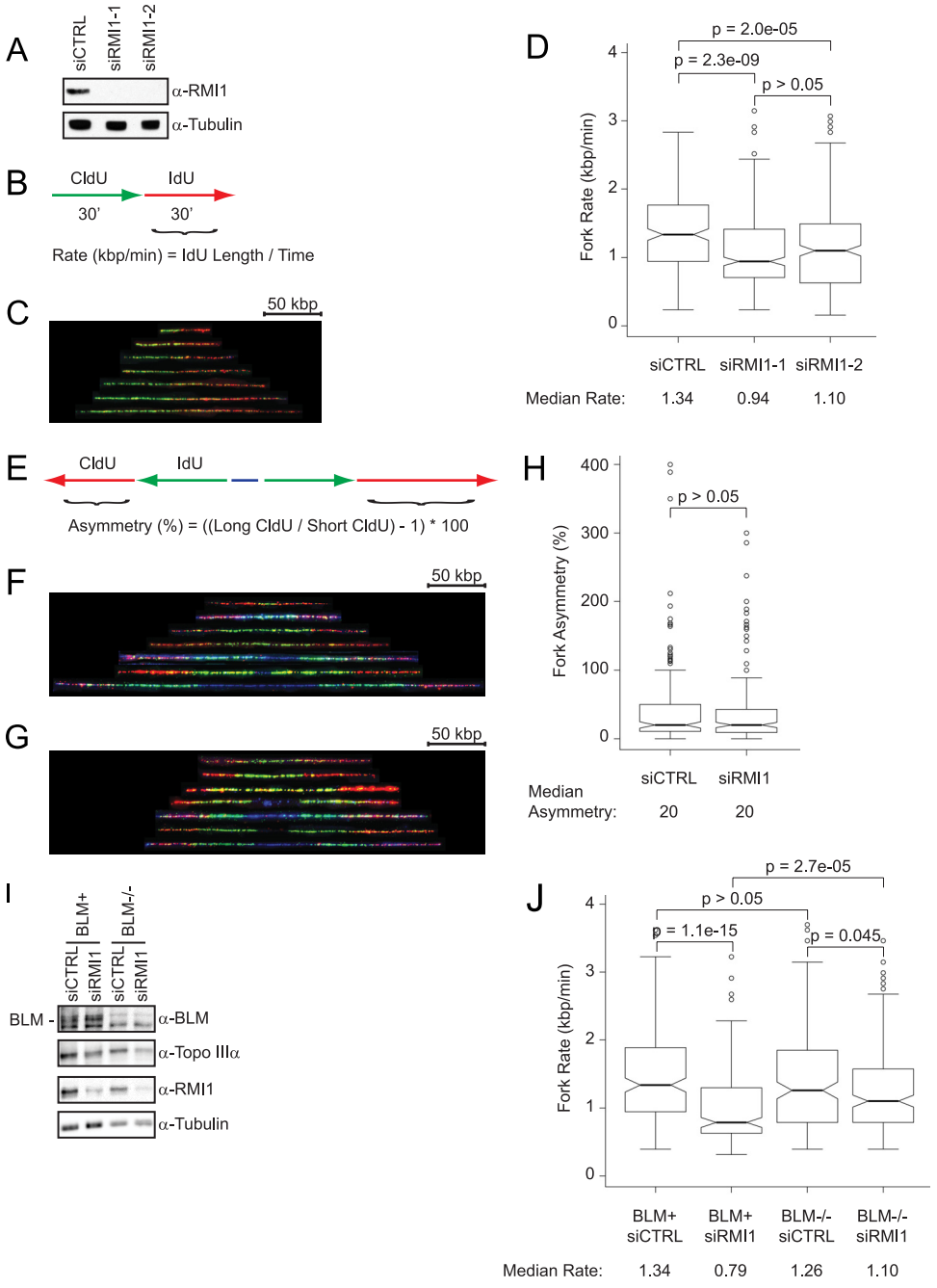

FIG 3 RMI1-depleted U2OS cells show a replication fork progression defect. (A) Extracts from U2OS cells transfected with siCTRL, siRMI1-1, or siRMI1-2 oligonucleotides for 48 h were subjected to immunoblotting analysis, probing for RMI1. An antitubulin antibody was included as a loading control. (B) Schematic diagram of a molecular combing experiment to determine the rate of replication fork progression. (C) Representative chromosome fibers used for replication fork progression analysis. The image is assembled from fibers on different micrographs following the extraction of fibers from the nonfiber background using Photoshop. A scale bar of 50 kbp is indicated at the top. (D) Distributions of the rates of replication fork progression in U2OS cells transfected with siCTRL, siRMI1-1, or siRMI1-2 oligonucleotides are represented in a box plot. The median fork rate for each experiment is shown. *P* values were determined by a two-tailed Mann-Whitney U test to compare the distributions of fork rates between two samples. (E) Schematic diagram of a molecular combing experiment to determine the degree of asymmetry in a bidirectional replication fork. (F and G) Representative chromosome fibers displaying symmetrical (F) or asymmetrical (G) bidirectional replication forks. The images are assembled from fibers on different micrographs following the extraction of fibers from the nonfiber background using Photoshop. A scale bar of 50 kbp is indicated at the top. (H) Distributions of the degrees of asymmetry of bidirectional replication forks in U2OS cells transfected with siCTRL or siRMI1 oligonucleotides are represented in a box plot. The median degree of asymmetry for each experiment is shown. The *P* value was determined by a two-tailed Mann-Whitney U test to compare the distributions of the degrees of fork asymmetry between two samples. (I) Extracts from PSNF5 (BLM^+) or PSNG13 ($BLM^{-/-}$) cells transfected with siCTRL or siRMI1 oligonucleotides were subjected to immunoblotting analysis, probing for BLM, TopoIIIα, and RMI1. An antitubulin antibody was included as a loading control. (J) Distributions of the rates of replication fork progression in PSNF5 (BLM^+) or PSNG13 ($BLM^{-/-}$) cells transfected with siCTRL or siRMI1 oligonucleotides are represented in a box plot. The median fork rate for each experiment is shown. *P* values were determined by a two-tailed Mann-Whitney U test to compare the distributions of fork rates between two samples.

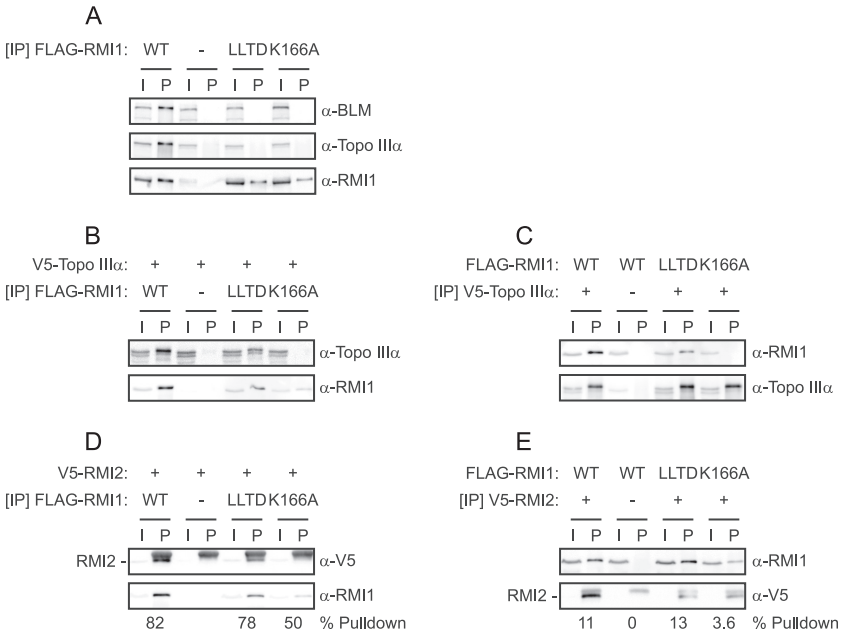

FIG 4 RMI1-LLTD and -K166A mutants are defective in binding to the BLM complex. (A) Extracts from cells expressing the indicated epitope-tagged proteins were immunoprecipitated (IP) with an anti-FLAG antibody to precipitate the FLAG-tagged RMI1 protein variants. Ten percent of the input extracts (I) and the precipitate (P) were fractionated on SDS-PAGE gels. Immunoblots were probed with anti-BLM, anti-TopoIIIα, and anti-RMI1 antibodies. (B) Extracts from cells expressing the indicated epitope-tagged proteins were immunoprecipitated with an anti-FLAG antibody to precipitate the FLAG-tagged RMI1 protein variants. Ten percent of the input extracts and the precipitate were fractionated on SDS-PAGE gels. Immunoblots were probed with anti-TopoIIIα and anti-RMI1 antibodies. (C) Extracts from cells expressing the indicated epitope-tagged proteins were immunoprecipitated with an anti-V5 antibody to precipitate V5-tagged TopoIIIα. Ten percent of the input extracts and the precipitate were fractionated on SDS-PAGE gels. Immunoblots were probed with anti-TopoIIIα and anti-RMI1 antibodies. (D) Extracts from cells expressing the indicated epitope-tagged proteins were immunoprecipitated with an anti-FLAG antibody to precipitate the FLAG-tagged RMI1 protein variants. Ten percent of the input extracts and the precipitate were fractionated on SDS-PAGE gels. Immunoblots were probed with an anti-V5 antibody to detect C-terminally V5-tagged RMI2 or with an anti-RMI1 antibody. The amount of RMI2 relative to that of RMI1 in the precipitate was calculated as a percentage and is indicated below the immunoblot. (E) Extracts from cells expressing the indicated epitope-tagged proteins were immunoprecipitated with an anti-V5 antibody to precipitate the RMI2 protein variants. Ten percent of the input extracts and the precipitate were fractionated on SDS-PAGE gels. Immunoblots were probed with an anti-V5 antibody to detect RMI2-V5 or with an anti-RMI1 antibody. The amount of RMI1 in the precipitate relative to that in the input extracts was calculated as a percentage and is indicated below the immunoblot. WT, wild type.

TopoIIIα binding, we focused on the RMI1-K166A mutant to study how complex formation contributes to RMI1 functions.

The RMI1-K166A mutant fails to form nuclear foci during replication fork stress. The results from coimmunoprecipitation experiments prompted us to investigate the ability of the RMI1-K166A mutant to form nuclear foci. We generated U2OS stable cell lines that expressed GFP-RMI1 variants containing eight silent mutations that make them resistant to siRMI1 treatment (see Fig. S5A and B in the supplemental material). Using these cell lines, we found that the K166A mutation resulted in at least a 5-fold reduction in the numbers of RMI1 nuclear foci in the presence of HU or aphidicolin (Fig. 5A and B), indicating that the ability of RMI1 to interact with BLM and TopoIIIα is crucial for RMI1 to respond to replication fork stress.

Reduced TopoIIIα protein level in the RMI1-K166A mutant. Previous studies have shown that the siRNA depletion of RMI1 reduces the TopoIIIα protein level (59), suggesting that complex formation between RMI1 and TopoIIIα is crucial for the maintenance of protein expression. We tested this directly by analyzing TopoIIIα protein levels in U2OS stable cell lines that expressed siRMI1-resistant RMI1 variants (Fig. 5C). We depleted endogenous RMI1 by siRNA treatment before inducing the expression of GFP, GFP-RMI1, or GFP–RMI1-K166A. The TopoIIIα protein level was reduced by more than 50% in cells depleted of endogenous RMI1 (Fig. 5C, lane 1 versus 2) but was restored upon the expression of GFP-RMI1 (Fig. 5C, lane 1 versus 4). Interestingly, the expression of GFP–RMI1-K166A was unable to restore TopoIIIα protein levels (Fig. 5C, lane 2 versus 6). The BLM protein level was unaffected under all experimental conditions. Together, these data indicate that BLM-TopoIIIα-RMI1 complex formation is a prerequisite for the stable expression of TopoIIIα but not of BLM.

The RMI1-K166A mutant disrupts BLM focus formation. BLM nuclear focus formation in mitomycin C was disrupted in cells depleted of RMI1 (59), suggesting a model in which BLM accumulation at DNA damage sites is dependent on RMI1. To test this idea further, we asked whether the RMI1-K166A mutant could support BLM nuclear focus formation. We depleted endogenous RMI1 by siRNA knockdown in U2OS stable cell lines that expressed siRMI1-resistant GFP, GFP-RMI1, or GFP–RMI1-K166A. We observed BLM nuclear foci in cells expressing GFP-RMI1 but not in those expressing GFP alone (Fig. 5D and E, and see Fig. S6A in the supplemental material), indicating that GFP-RMI1 is able to support BLM nuclear focus formation. In contrast, the percentage of cells harboring BLM nuclear foci decreased dramatically in cells expressing GFP–RMI1-K166A, to the level seen for cells expressing GFP alone. Importantly, the reduction in numbers of BLM nuclear foci was not due to changes in BLM

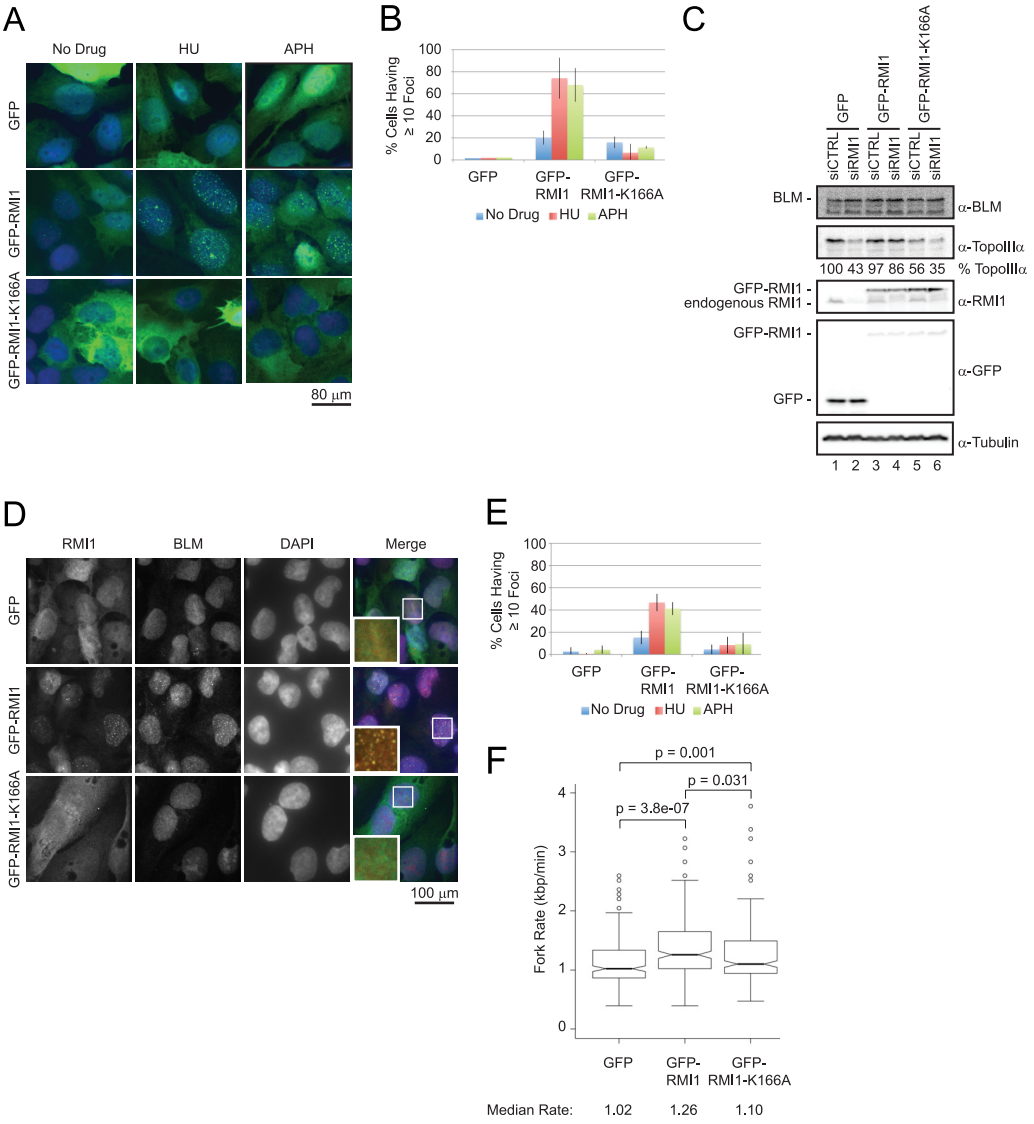

FIG 5 The RMI1-K166A mutant is defective in nuclear focus formation and does not support BLM nuclear focus formation. (A) Representative confocal microscopy images are shown, to visualize GFP, GFP-RMI1, or GFP–RMI1-K166A (green) in the nucleus (blue) (DAPI) in cells treated with no drug, 4 mM HU, or 30 μM aphidicolin for 24 h. Note that there was no siRNA treatment; therefore, endogenous RMI1 was present in all cases. (B) Images from the experiment in panel A were analyzed to determine the percentage of cells with more than 10 nuclear foci. (C) U2OS stable cell lines that express GFP, GFP-RMI1, or GFP–RMI1-K166A were treated with siCTRL or siRMI1 oligonucleotides for 48 h. Extracts were subjected to immunoblotting analysis to probe for BLM, TopoIIIα, and RMI1 protein levels. An anti-GFP antibody was included to distinguish GFP-RMI1 from endogenous RMI1 protein levels. An antitubulin antibody was included as a loading control. (D) U2OS stable cell lines that express GFP, GFP-RMI1, or GFP–RMI1-K166A were transfected with the siRMI1 oligonucleotide for 24 h before being treated with no drug, 4 mM HU, or 30 μM aphidicolin for an additional 24 h. Indirect immunofluorescence analysis using an anti-BLM antibody was performed to visualize RMI1 (green) or BLM (red) foci in the nucleus (blue) (DAPI). (E) Images from the experiment depicted in panel D were analyzed to determine the percentage of cells with more than 10 BLM nuclear foci. (F) Distributions of the rates of replication fork progression in U2OS cells that express GFP, GFP-RMI1, or GFP–RMI1-K166A are represented in a box plot. The median fork rate for each experiment is shown. *P* values were determined by a two-tailed Mann-Whitney U test to compare the distributions of fork rates between two samples.

abundance (Fig. 5C, lane 2 versus 4 versus 6). Together, these data indicate that BLM-TopoIIIα-RMI1 complex formation is crucial in driving the recruitment of BLM to nuclear foci.

The RMI1-K166A mutant shows a replication fork progression defect. We asked whether the role of RMI1 in promoting normal replication fork progression requires BLM complex formation. We repeated the molecular combing experiment with U2OS stable cell lines that were depleted of endogenous RMI1 by siRNA treatment while expressing siRNA-resistant GFP, GFP-RMI1, or GFP–RMI1-K166A. The expression of siRNA-resistant GFP-RMI1 resulted in a significant, but not complete, suppression of the fork progression defect caused by the depletion of endogenous RMI1 (Fig. 5F, and see Fig. S6B in the supplemental material). We found that cells that expressed GFP–RMI1-K166A (1.10 kbp/min) exhibited an intermediate fork rate between those that expressed GFP (1.02 kbp/min; $P = 0.001$) and those that expressed GFP-RMI1 (1.26 kbp/min; $P = 0.03$) (Fig. 5F). These data suggest that BLM complex formation is important, but per-

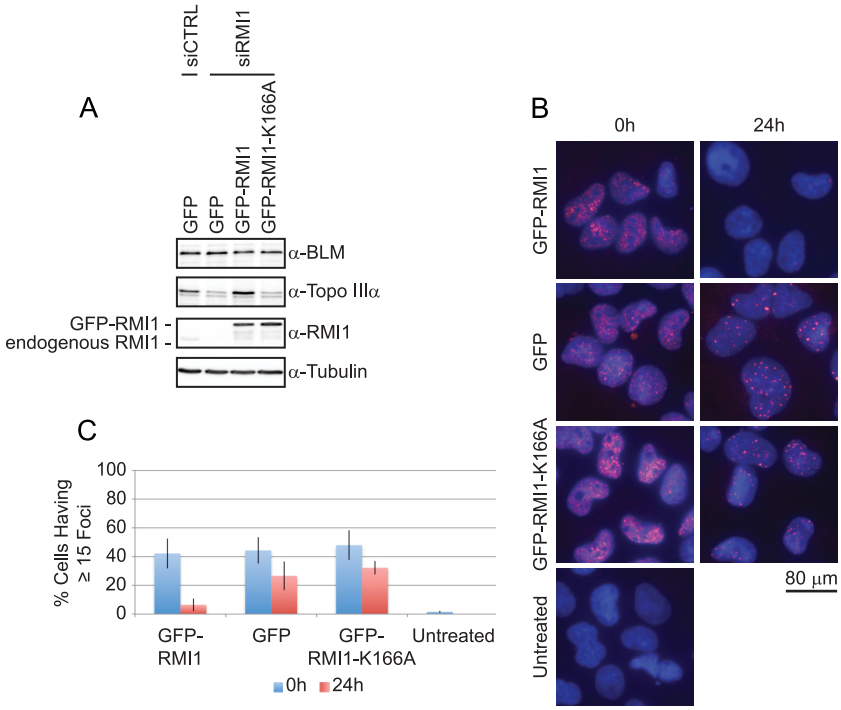

FIG 6 U2OS cells that express the RMI1-K166A mutant display persistent γH2AX foci after aphidicolin treatment. (A) U2OS stable cell lines that express GFP, GFP-RMI1 or GFP–RMI1-K166A were transfected with the siRMI1 oligonucleotide for 48 h. Afterwards, cells were treated with 30 μM aphidicolin for 6 h before recovery in drug-free medium for an additional 24 h. Extracts were subjected to immunoblotting analysis after recovery, probing for BLM, TopoIIIα, and RMI1 protein levels. An antitubulin antibody was included as a loading control. (B) U2OS stable cell lines that express GFP, GFP-RMI1, or GFP–RMI1-K166A were transfected with the siRMI1 oligonucleotide and grown for 48 h. Cells were then treated with 30 μM aphidicolin for 6 h before recovery in drug-free medium for an additional 24 h. Representative confocal microscopy images are shown, to visualize γH2AX (red) in the nucleus (blue) (DAPI) at 0 and 24 h after the removal of aphidicolin. Cells that were not treated with aphidicolin were included as a control for the background level of γH2AX foci. (C) Images from the experiment depicted in panel A were analyzed to determine the percentage of cells with more than 15 γH2AX nuclear foci.

haps not essential, for RMI1 to promote normal replication fork progression.

RMI1 is required for recovery from aphidicolin-mediated replication fork stress. Our data indicate that the binding of RMI1 to BLM and TopoIIIα is critical for the formation of BLM-TopoIIIα-RMI1 nuclear foci in response to replication fork stress. We asked whether RMI1 foci correlated with improved recovery from aphidicolin-induced replication fork stress. We knocked down endogenous RMI1 in U2OS stable cell lines that expressed siRMI1-resistant GFP, GFP-RMI1, or GFP–RMI1-K166A (Fig. 6A). We then treated these cells with 30 μM aphidicolin for 6 h before recovery in aphidicolin-free medium for an additional 24 h. Since γH2AX localizes to nuclear foci at sites of DNA strand breaks (41), we measured the persistence of γH2AX nuclear foci as an indicator of the presence of unrepaired DNA damage. Immediately after the removal of replication stress (0 h of recovery), more than 40% of cells in all cell lines exhibited at least 15 γH2AX nuclear foci, consistent with previous reports that replication arrest induces histone H2AX phosphorylation and subnuclear localization (52). After 24 h of recovery, these nuclear foci disappeared in cells that expressed GFP-RMI1 but not in those that expressed GFP alone, indicating that RMI1 is necessary for recovery from aphidicolin-induced replication fork stress (Fig. 6B and C). Interestingly, cells that expressed the GFP–RMI1-K166A mutant exhibited elevated numbers of γH2AX nuclear foci at a level similar to those that expressed GFP alone 24 h after recovery. These data suggest that the localization of RMI1 to nuclear foci is a critical step in promoting the repair of DNA damage that results from DNA replication fork stress.

DISCUSSION

RMI1 is important for the optimal strand passage activity of BLM-TopoIIIα *in vitro* (38, 54, 58). Strand passage activity is likely critical for a number of cellular processes during DNA replication and repair in which Holliday junctions feature. Here we have investigated the role of RMI1 in DNA replication *in vivo*. We found that RMI forms nuclear foci with BLM and TopoIIIα in unperturbed cells and that the abundance of these foci increased during replication stress. Cells depleted of RMI1 exhibited a reduced replication fork rate, which was alleviated in the absence of BLM, suggesting that RMI1 functions downstream of BLM in promoting normal replication fork progression. In the absence of RMI1, cells were defective in recovery from aphidicolin-induced DNA damage, and a proper response to replication fork stress required a physical interaction between RMI1, BLM, and TopoIIIα. Together, these data indicate that RMI1 functions in normal DNA replication progression and with the RMI1 binding partner BLM and that TopoIIIα mediates recovery from replication fork stress.

RMI1 functions as a complex with BLM and TopoIIIα *in vivo*. Biochemical analyses have demonstrated that RMI1 is essential for the optimal activities of BLM and TopoIIIα *in vitro* (5, 54, 58), suggesting the importance of complex formation for cellular activities. Here we provide evidence that BLM, TopoIIIα, and RMI1 function as a complex *in vivo*. First, BLM, TopoIIIα, and

RMI1 nuclear foci colocalize with one another. Second, nuclear focus formation by BLM, TopoIIIα, and RMI1 was interdependent. Last, the RMI1 mutant that was defective in binding to BLM and TopoIIIα did not support BLM complex nuclear focus formation. Therefore, we propose that BLM, TopoIIIα, and RMI1 exist as a complex *in vivo* and that recruitment to subnuclear foci occurs simultaneously instead of sequentially.

RMI1 promotes normal DNA replication fork progression. Using single-molecule analysis of two different cell lines, we provide direct evidence that RMI1 is involved in promoting replication fork progression, as cells that lacked RMI1 exhibited reduced replication fork rates. The replication defect that we observed is not likely an indirect effect of RMI1 depletion on BLM protein levels, as these remained at wild-type levels. Rather, we propose that the depletion of RMI1 impacts either the DNA helicase activity of BLM (which RMI1 stimulates [5]), the decatenase activity of TopoIIIα (which RMI1 stimulates [58]), or the DHJ dissolution activity of the BLM-TopoIIIα-RMI1 complex (38, 54), but note that none of these possibilities are mutually exclusive. DNA replication defects during an unperturbed S phase could account for the reduced viability and increased numbers of SCEs in cells depleted of RMI1 (59). Given the emerging role of DNA replication stress in early stages of oncogenesis (22), it is possible that the increased risk of acute myeloid leukemia associated with mutations in RMI1 (4) is the result of the DNA replication fork defects that we detected when RMI1 was depleted.

Of particular interest, we find evidence that the role of RMI1 in DNA replication is distinct from that of BLM. The decrease in the replication fork rate that we detected by DNA combing was greater in cells depleted of RMI1 than in $BLM^{-/-}$ cells. Additionally, BS cells exhibit an elevated frequency of fork pausing associated with a low replication rate (36), consistent with dual roles in maintaining replication progression and preventing the collapse of stalled replication forks (1). We did not observe an elevated frequency of fork pausing in RMI1-depleted cells, suggesting that RMI1 is not directly involved in stabilizing stalled replication forks and providing further evidence that the replication defects that we observed following RMI1 depletion are not due to BLM dysfunction. Finally, the deletion of BLM suppressed the replication defect in RMI1 knockdown cells, again indicating that BLM and RMI1 are functionally distinct. Since BLM failed to form subnuclear foci in RMI1 knockdown cells, these data also indicate that the inhibition of fork progression that we observed following RMI1 depletion depends on BLM but not on the formation of BLM-TopoIIIα-RMI1 subnuclear foci.

Genes that are involved in homologous recombination, RAD51, XRCC2, and BRCA2, are involved in a general modulation of replication elongation rather than a localized rescue of stalled forks (14), much like RMI1. RAD51 and BRCA2 promote replication progression by preventing the accumulation of ssDNA gaps and protecting nascent DNA from MRE11-mediated degradation, an S-phase-specific role that is independent of DSB repair (23, 42). Given that RMI1 also participates in homologous recombination at the resolution steps, it is possible that RMI1 promotes replication fork progression during elongation in a manner similar to that of RAD51 and BRCA2.

The BLM-TopoIIIα-RMI1 interaction is critical for the DNA replication stress response. RMI1 foci, which colocalize with BLM and with TopoIIIα foci, showed a dramatic increase in abundance in the presence of the replication inhibitor HU or aphidicolin, indicating that RMI1 functions with BLM and TopoIIIα during replication stress *in vivo*. By mutating lysine 166 of RMI1, which is required for the proper folding of the RMI1 N terminus (50) and for TopoIIIα-RMI1 interactions *in vitro* (39, 58), we found that lysine 166 is essential for BLM and TopoIIIα interactions *in vivo*. We were able to probe the importance of these interactions for RMI1 subcellular localization and function. The RMI1-K166A protein failed to form nuclear foci following aphidicolin treatment, indicating that complex formation is necessary for proper RMI1 localization in response to replication stress. When we analyzed γH2AX, we found that DNA damage resulting from replication stress persisted in the absence of RMI1. DNA damage persistence was not rescued by the expression of the RMI1-K166A mutant, indicating that the physical interaction of RMI1 with BLM and TopoIIIα is essential for RMI1 to promote recovery from DNA replication stress *in vivo*. This agrees well with data from previous biochemical studies which found that the interaction between BLM, TopoIIIα, and RMI1 is important for the role of RMI1 in stimulating the decatenase activity of TopoIIIα (58) and the DHJ dissolution activity of BLM-TopoIIIα (39, 58). We therefore hypothesize that the inability of the RMI1-K166A mutant to localize to subnuclear foci with BLM and TopoIIIα leads to compromised BLM-TopoIIIα activity in resolving recombination intermediates that arise during replication stress and results in the persistence of DNA damage. However, it is interesting that the RMI1-K166A mutant also compromised the localization of BLM to nuclear foci following replication stress, suggesting that the BLM subnuclear localization is also dependent on complex formation. Given that BLM also participates in recovery from replication stress, we envision a scenario in which a failure to recruit BLM to repair foci contributes to the persistence of aphidicolin-induced DNA damage in cells that express the RMI1-K166A mutant. Together, these data indicate the importance of BLM-TopoIIIα-RMI1 complex formation *in vivo* and indicate that just as complex formation is required for robust enzymatic function *in vitro*, it is required for the response to replication stress *in vivo*.

ACKNOWLEDGMENTS

We thank Ian Hickson, Laurence Pelletier, and Weidong Wang for antibody reagents and Philippe Pasero, Etienne Schwob, Christopher Yip, and Michael Lee for assistance with molecular combing.

L.O. holds a postdoctoral fellowship from the Canadian Breast Cancer Foundation. This work was supported by Canadian Institutes of Health Research grants MOP-79368 (to G.W.B.) and MOP-84297 (to D.D.).

REFERENCES

1. **Bachrati CZ, Hickson ID.** 2008. RecQ helicases: guardian angels of the DNA replication fork. Chromosoma **117**:219–233.
2. **Bensimon A, et al.** 1994. Alignment and sensitive detection of DNA by a moving interface. Science **265**:2096–2098.
3. **Branzei D, Foiani M.** 2009. The checkpoint response to replication stress. DNA Repair (Amst.) **8**:1038–1046.
4. **Broberg K, et al.** 2007. Genetic variant of the human homologous recombination-associated gene RMI1 (S455N) impacts the risk of AML/MDS and malignant melanoma. Cancer Lett. **258**:38–44.
5. **Bussen W, Raynard S, Busygina V, Singh AK, Sung P.** 2007. Holliday junction processing activity of the BLM-Topo IIIalpha-BLAP75 complex. J. Biol. Chem. **282**:31484–31492.
6. **Cejka P, Plank JL, Bachrati CZ, Hickson ID, Kowalczykowski SC.** 2010. Rmi1 stimulates decatenation of double Holliday junctions during dissolution by Sgs1-Top3. Nat. Struct. Mol. Biol. **17**:1377–1382.
7. **Chaganti RS, Schonberg S, German J.** 1974. A manyfold increase in sister chromatid exchanges in Bloom's syndrome lymphocytes. Proc. Natl. Acad. Sci. U. S. A. **71**:4508–4512.

8. **Champoux JJ.** 2001. DNA topoisomerases: structure, function, and mechanism. Annu. Rev. Biochem. **70**:369–413.
9. **Champoux JJ.** 2002. Type IA DNA topoisomerases: strictly one step at a time. Proc. Natl. Acad. Sci. U. S. A. **99**:11998–12000.
10. **Chang M, et al.** 2005. RMI1/NCE4, a suppressor of genome instability, encodes a member of the RecQ helicase/Topo III complex. EMBO J. **24**: 2024–2033.
11. **Cobb JA, et al.** 2005. Replisome instability, fork collapse, and gross chromosomal rearrangements arise synergistically from Mec1 kinase and RecQ helicase mutations. Genes Dev. **19**:3055–3069.
12. **Conti C, Caburet S, Schurra C, Bensimon A.** 2001. Molecular combing. Curr. Protoc. Cytom. **8**:8.10.
13. **Conti C, et al.** 2007. Replication fork velocities at adjacent replication origins are coordinately modified during DNA replication in human cells. Mol. Biol. Cell **18**:3059–3067.
14. **Daboussi F, et al.** 2008. A homologous recombination defect affects replication-fork progression in mammalian cells. J. Cell Sci. **121**:162–166.
15. **Davalos AR, Campisi J.** 2003. Bloom syndrome cells undergo p53-dependent apoptosis and delayed assembly of BRCA1 and NBS1 repair complexes at stalled replication forks. J. Cell Biol. **162**:1197–1209.
16. **Davalos AR, Kaminker P, Hansen RK, Campisi J.** 2004. ATR and ATM-dependent movement of BLM helicase during replication stress ensures optimal ATM activation and 53BP1 focus formation. Cell Cycle **3**:1579–1586.
17. **Davies SL, North PS, Dart A, Lakin ND, Hickson ID.** 2004. Phosphorylation of the Bloom's syndrome helicase and its role in recovery from S-phase arrest. Mol. Cell. Biol. **24**:1279–1291.
18. **Davies SL, North PS, Hickson ID.** 2007. Role for BLM in replication-fork restart and suppression of origin firing after replicative stress. Nat. Struct. Mol. Biol. **14**:677–679.
19. **Gangloff S, McDonald JP, Bendixen C, Arthur L, Rothstein R.** 1994. The yeast type I topoisomerase Top3 interacts with Sgs1, a DNA helicase homolog: a potential eukaryotic reverse gyrase. Mol. Cell. Biol. **14**:8391–8398.
20. **Gaymes TJ, et al.** 2002. Increased error-prone non homologous DNA end-joining—a proposed mechanism of chromosomal instability in Bloom's syndrome. Oncogene **21**:2525–2533.
21. **German J.** 1995. Bloom's syndrome. Dermatol. Clin. **13**:7–18.
22. **Halazonetis TD, Gorgoulis VG, Bartek J.** 2008. An oncogene-induced DNA damage model for cancer development. Science **319**:1352–1355.
23. **Hashimoto Y, Chaudhuri AR, Lopes M, Costanzo V.** 2010. Rad51 protects nascent DNA from Mre11-dependent degradation and promotes continuous DNA synthesis. Nat. Struct. Mol. Biol. **17**:1305–1311.
24. **Hickson ID.** 2003. RecQ helicases: caretakers of the genome. Nat. Rev. Cancer **3**:169–178.
25. **Hoadley KA, et al.** 2010. Structure and cellular roles of the RMI core complex from the bloom syndrome dissolvasome. Structure **18**:1149–1158.
26. **Hu P, et al.** 2001. Evidence for BLM and topoisomerase IIIalpha interaction in genomic stability. Hum. Mol. Genet. **10**:1287–1298.
27. **Hyrien O.** 2000. Mechanisms and consequences of replication fork arrest. Biochimie **82**:5–17.
28. **Lambert S, Froget B, Carr AM.** 2007. Arrested replication fork processing: interplay between checkpoints and recombination. DNA Repair (Amst.) **6**:1042–1061.
29. **Mankouri HW, Hickson ID.** 2007. The RecQ helicase-topoisomerase III-Rmi1 complex: a DNA structure-specific 'dissolvasome'? Trends Biochem. Sci. **32**:538–546.
30. **Mao FJ, Sidorova JM, Lauper JM, Emond MJ, Monnat RJ.** 2010. The human WRN and BLM RecQ helicases differentially regulate cell proliferation and survival after chemotherapeutic DNA damage. Cancer Res. **70**:6548–6555.
31. **Mullen JR, Nallaseth FS, Lan YQ, Slagle CE, Brill SJ.** 2005. Yeast Rmi1/Nce4 controls genome stability as a subunit of the Sgs1-Top3 complex. Mol. Cell. Biol. **25**:4476–4487.
32. **Myung K, Datta A, Chen C, Kolodner RD.** 2001. SGS1, the Saccharomyces cerevisiae homologue of BLM and WRN, suppresses genome instability and homeologous recombination. Nat. Genet. **27**:113–116.
33. **Petermann E, Helleday T.** 2010. Pathways of mammalian replication fork restart. Nat. Rev. Mol. Cell Biol. **11**:683–687.
34. **Plank J, Hsieh TS.** 2009. Helicase-appended topoisomerases: new insight into the mechanism of directional strand transfer. J. Biol. Chem. **284**: 30737–30741.
35. **Plank JL, Wu J, Hsieh TS.** 2006. Topoisomerase IIIalpha and Bloom's helicase can resolve a mobile double Holliday junction substrate through convergent branch migration. Proc. Natl. Acad. Sci. U. S. A. **103**:11118–11123.
36. **Rao VA, et al.** 2007. Endogenous gamma-H2AX-ATM-Chk2 checkpoint activation in Bloom's syndrome helicase deficient cells is related to DNA replication arrested forks. Mol. Cancer Res. **5**:713–724.
37. **Rassool FV, North PS, Mufti GJ, Hickson ID.** 2003. Constitutive DNA damage is linked to DNA replication abnormalities in Bloom's syndrome cells. Oncogene **22**:8749–8757.
38. **Raynard S, Bussen W, Sung P.** 2006. A double Holliday junction dissolvasome comprising BLM, topoisomerase IIIalpha, and BLAP75. J. Biol. Chem. **281**:13861–13864.
39. **Raynard S, et al.** 2008. Functional role of BLAP75 in BLM-topoisomerase IIIalpha-dependent Holliday junction processing. J. Biol. Chem. **283**: 15701–15708.
40. **Rodriguez-Lopez AM, Jackson DA, Iborra F, Cox LS.** 2002. Asymmetry of DNA replication fork progression in Werner's syndrome. Aging Cell **1**:30–39.
41. **Rogakou EP, Pilch DR, Orr AH, Ivanova VS, Bonner WM.** 1998. DNA double-stranded breaks induce histone H2AX phosphorylation on serine 139. J. Biol. Chem. **273**:5858–5868.
42. **Schlacher K, et al.** 2011. Double-strand break repair-independent role for BRCA2 in blocking stalled replication fork degradation by MRE11. Cell **145**:529–542.
43. **Selak N, et al.** 2008. The Bloom's syndrome helicase (BLM) interacts physically and functionally with p12, the smallest subunit of human DNA polymerase delta. Nucleic Acids Res. **36**:5166–5179.
44. **Sharma S, et al.** 2004. Stimulation of flap endonuclease-1 by the Bloom's syndrome protein. J. Biol. Chem. **279**:9847–9856.
45. **Singh TR, et al.** 2008. BLAP18/RMI2, a novel OB-fold-containing protein, is an essential component of the Bloom helicase-double Holliday junction dissolvasome. Genes Dev. **22**:2856–2868.
46. **Stewart GS, et al.** 2009. The RIDDLE syndrome protein mediates a ubiquitin-dependent signaling cascade at sites of DNA damage. Cell **136**:420–434.
47. **Suski C, Marians KJ.** 2008. Resolution of converging replication forks by RecQ and topoisomerase III. Mol. Cell **30**:779–789.
48. **Tercero JA, Diffley JF.** 2001. Regulation of DNA replication fork progression through damaged DNA by the Mec1/Rad53 checkpoint. Nature **412**: 553–557.
49. **Tuduri S, et al.** 2009. Topoisomerase I suppresses genomic instability by preventing interference between replication and transcription. Nat. Cell Biol. **11**:1315–1324.
50. **Wang F, et al.** 2010. Crystal structures of RMI1 and RMI2, two OB-fold regulatory subunits of the BLM complex. Structure **18**:1159–1170.
51. **Wang W, Bambara RA.** 2005. Human Bloom protein stimulates flap endonuclease 1 activity by resolving DNA secondary structure. J. Biol. Chem. **280**:5391–5399.
52. **Ward IM, Chen J.** 2001. Histone H2AX is phosphorylated in an ATR-dependent manner in response to replicational stress. J. Biol. Chem. **276**: 47759–47762.
53. **Watt PM, Hickson ID, Borts RH, Louis EJ.** 1996. SGS1, a homologue of the Bloom's and Werner's syndrome genes, is required for maintenance of genome stability in Saccharomyces cerevisiae. Genetics **144**:935–945.
54. **Wu L, et al.** 2006. BLAP75/RMI1 promotes the BLM-dependent dissolution of homologous recombination intermediates. Proc. Natl. Acad. Sci. U. S. A. **103**:4068–4073.
55. **Wu L, Hickson ID.** 2003. The Bloom's syndrome helicase suppresses crossing over during homologous recombination. Nature **426**:870–874.
56. **Xu D, et al.** 2008. RMI, a new OB-fold complex essential for Bloom syndrome protein to maintain genome stability. Genes Dev. **22**:2843–2855.
57. **Yamagata K, et al.** 1998. Bloom's and Werner's syndrome genes suppress hyperrecombination in yeast sgs1 mutant: implication for genomic instability in human diseases. Proc. Natl. Acad. Sci. U. S. A. **95**:8733–8738.
58. **Yang J, Bachrati CZ, Ou J, Hickson ID, Brown GW.** 2010. Human topoisomerase IIIalpha is a single-stranded DNA decatenase that is stimulated by BLM and RMI1. J. Biol. Chem. **285**:21426–21436.
59. **Yin J, et al.** 2005. BLAP75, an essential component of Bloom's syndrome protein complexes that maintain genome integrity. EMBO J. **24**:1465–1476.